Journal of Peptide Science
J. Pept. Sci. 2008; **14**: 85–96
Published online 8 October 2007 in Wiley InterScience (www.interscience.wiley.com). DOI: 10.1002/psc.917

JOURNAL OF PEPTIDE SCIENCE

Conformational studies of vasopressin and mesotocin using NMR spectroscopy and molecular modelling methods. Part II: studies in the SDS micelle

SYLWIA RODZIEWICZ-MOTOWIDŁO,[a]* EMILIA SIKORSKA,[a] MARTA OLESZCZUK[b,c] and CEZARY CZAPLEWSKI[a]

[a] Faculty of Chemistry, University of Gdańsk, Sobieskiego 18, 80-952 Gdańsk, Poland
[b] Laboratory of Biological NMR, Institute of Biochemistry and Biophysics, PAS, Pawińskiego 5a, 02-106 Warsaw, Poland
[c] Department of Biochemistry, University of Alberta, Edmonton, Alberta, Canada T6G 2H7CA, Canada

Received 5 June 2007; *Accepted 12 July 2007*

Abstract: There is much evidence to support the hypothesis that lipids play a role in the interaction of peptide hormones with their membrane receptors. This interaction through change of peptide conformation can facilitate the entry of the hormone into the microenvironment of the receptor. In the present study we have examined the interaction of vasopressin and mesotocin with a lipid – sodium dodecylsulfate (SDS) micelle – using 2D nuclear magnetic resonance (NMR) and theoretical methods. Solution structures of two hormones in solution with SDS were established using the nuclear Overhauser effect (NOE) and the $^{3}J_{NHH\alpha}$ couplings. The amino acid sequences of these peptides are: c[C^{1}-Y^{2}-F^{3}-Q^{4}-N^{5}-C^{6}]-P^{7}-R^{8}-G^{9}-NH$_2$ ([Arg^{8}]vasopressin, AVP) and c[C^{1}-Y^{2}-I^{3}-Q^{4}-N^{5}-C^{6}]-P^{7}-I^{8}-G^{9}-NH$_2$ (MT). Each of the peptides was found to occur as one stable conformation. AVP adopts the *cis* configuration on the Cys^{1}-Tyr^{2} peptide bond, a finding not reported so far. The three-dimensional structures of the two peptides studied were determined by a method that consisted of time-averaged molecular dynamics in *an explicit* SDS micelle with the parm99 force field in AMBER8.0 package. All calculated structures of the studied peptides form β-turns in their cyclic parts. The *C*-terminal fragment of MT is bent, whereas that of AVP is extended. Copyright © 2007 European Peptide Society and John Wiley & Sons, Ltd.

Keywords: mesotocin (MT); molecular dynamics; NMR; SDS micelle; time-averaged (TAV); vasopressin (AVP)

INTRODUCTION

Till now, 13 vertebrate neurohypophyseal hormones and 6 invertebrate [1] neurohypophyseal hormone-like peptides are known. These neurohypophyseal hormones are usually nonapeptides that exhibit several highly conserved residues such as the half-cystine residues at positions 1 and 6 that form a disulfide bridge, the tyrosine at position 2, the asparagine at position 5 and the proline residue at position 7. All of them possess an amide at the *C*-terminus.

The neurohypophyseal hormones used by most mammals are [Arg^{8}]vasopressin (AVP) and oxytocin (OT). The endogenous nonapeptide arginine vasopressin is a hormone with a broad spectrum of functions. It controls first of all urine concentration [2] and blood pressure [3,4]. Furthermore, it is responsible for stimulation of the adrenocorticotropine secretion [5] and stability of the body temperature [6]. It influences some social behavioral [7] and sexual reactions [8]. This hormone also causes nonopioid anti-pain effect [9] and drug addiction [10]. It is thought that the vasopressin may influence the higher functions as memorizing and learning [11]. OT contracts uterine smooth muscle during labor, influences mating behavior, and is responsible for the milk letdown reflex. Most species have a vasopressin-like hormone with a polar residue in position 8 (arginine or lysine in mammals) of the nonapeptide and an OT-like hormone with a nonpolar amino acid residue in position 8 (leucine in mammals). In amphibians, vasotocin ([Ile^{3}]vasopressin, VT) and mesotocin ([Ile^{8}]oxytocin, MT) represent these two subclasses. They function to regulate water balance in amphibia, such as frogs or toads. The hormones influence the urinary bladder and epidermis permeability to water and ions as well as the kidney during the control of the glomerular filtration rate. Whereas VT (like all the vasopressin-related peptides) functions as an antidiuretic agent, there is evidence that MT functions as a diuretic agent [12], possibly by antagonizing the actions of VT [13] and/or by increasing glomerular filtration [14,15]. Probably MT serves important neurotransmitter functions in addition to its hormonal role in water balance [16,17]. MT, which was originally identified in amphibians [18], was evolutionarily very stable, since it is present in all nonmammalian tetrapods investigated to date. It has been identified in lungfish, amphibians, reptiles, birds, and marsupials [19]. In this paper we investigate two hormones, vasopressin (AVP) and mesotocin (MT). There is a high degree of homology between arginine vasopressin c[Cys^{1}-Tyr^{2}-Phe^{3}-Gln^{4}-Asn^{5}-Cys^{6}]-Pro^{7}-Arg^{8}-Gly^{9}-NH$_2$ and mesotocin c[Cys^{1}-Tyr^{2}-Ile^{3}-Gln^{4}-Asn^{5}-Cys^{6}]-Pro^{7}

*Correspondence to: Sylwia Rodziewicz-Motowidło, Faculty of Chemistry, University of Gdańsk, Sobieskiego 18, 80-952 Gdańsk, Poland; e-mail: sylwia@chem.univ.gda.pl

-Ile^8-Gly^9-NH_2, but it is expedient to consider them separately because of their clearly divergent physiological activity, their different gene structure, and their different evolutionary lineages.

In aqueous solution, a small peptide does not adopt a stable structure but exists in many conformations in equilibrium. Vasopressin and mesotocin exist as well in conformational equilibrium in water solution (see Part I) [20]. Organic solvents, such as dimethyl sulfoxide or trifluoroethanol, which are often employed to study the impact of a membrane environment, restrict conformational freedom of the peptides. Micelles or liposomes provide a much better model of biological membranes. Moreover, they enable exploration of the influence of the lipid environment on peptide conformational properties, all the more because the current model for peptide hormone interactions with receptors suggests that the bioactive conformation of the peptide is induced upon the association with the cell membrane followed by a two-dimensional diffusion process, whereby the ligand is recognized and then interacts with the receptor [21,22].

In this paper we study the interactions of two nonapeptide hormones with membrane mimic by the concerted use of nuclear magnetic resonance (NMR) and restrained time-averaged molecular dynamics (MD) simulation techniques employing explicit (united-atom) membrane model. In our work the sodium dodecylsulfate (SDS) micelle was used as an economical and effective model for a membrane environment. Until now, only initial conformational studies, but without the 3D structure of AVP and OT, using CD and 1D NMR spectroscopy in SDS micelle have been reported [23]. The results indicated that both neurohypophyseal hormones interact with lipids by changing their conformations. Hydrophobic interactions between a lipid tail and hydrophobic core of peptides are responsible for such conformational changes. To date, there has been lack of data concerning conformational properties of MT, except using the Raman and the circular dichroism spectroscopies [24]. Therefore, it seems worthwhile to study the structure of the MT peptide.

MATERIALS AND METHODS

Sample Preparation

The peptides and SDS-d_{25} were purchased from Bachem AG. All the peptides were of >95% purity. The samples in the SDS micelles were prepared at a concentration of approximately 2 mg and 2.03 mg of AVP and MT, respectively, in 0.6 ml of the KH_2PO_4/Na_2HPO_4 buffer at pH ≈7, containing 55.1 mg and 52.0 mg of SDS-d_{25} for AVP and MT, respectively. The SDS-d_{25} : peptide ratio was adjusted to 1 : 100.

NMR Experiments

The NMR spectra were recorded on a 500-MHz Varian spectrometer equipped with a Performa II gradient generator unit, WFG, Ultrashims, high-stability temperature unit and a 5-mm $^1H\{^{13}C/^{15}N\}$ PFG triple resonance inverse probe head.

The 2D NMR spectra were measured at 28 °C in the SDS micelle. The temperature coefficients of the amide proton chemical shifts were measured from 1D NMR spectra for the following temperatures: 10, 15, 20, 25, 28, 30, 35, 40 and 45 °C. Proton resonance assignments were achieved by use of the proton–proton total chemical shift correlation spectroscopy (TOCSY) [25], the nuclear Overhauser effect spectroscopy (NOESY) [26], the rotating-frame Overhauser enhancement spectroscopy (ROESY) [27,28], as well as the gradient heteronuclear single quantum coherence ($^1H-^{13}C$ gHSQC, $^1H-^{15}N$ HSQC) [29,30] and the gradient heteronuclear multiple quantum coherence ($^1H-^{13}C$ gHMBC) techniques [31]. For each sample, the mixing time of 80 ms for TOCSY was measured. The NOESY spectra were recorded with mixing times of 200 and 400 ms. The mixing time of the ROESY experiments were set to 200 ms. The volumes of cross-peaks were picked up for micellar samples with a mixing time of 200 ms on the NOESY spectra.

All spectra were measured with water signal presaturation pulse typically of 2 dB and 1.5 s. In the case of the 1D NMR spectra, 16K data points were collected and a spectral width of 6 kHz was used. The 2D homonuclear experiments were measured using a proton spectral width of 4.5 kHz collecting 2K data points.

Vicinal coupling constants, $^3J_{NHH\alpha}$, were assigned using ACT-ct-COSY [32] and 1D NMR spectra. Unfortunately, broad correlation cross-peaks made it impossible to determine most of the vicinal coupling constants from the ACT-ct-COSY spectra. Thus, the values of the coupling constants were mostly read from the 1D NMR spectra at 28 °C.

The spectra were calibrated against a HOD signal, taking into account temperature drift of the reference signal given by the equation $\delta_{1H(T)} = 5.060 - 0.0122T + (2.11 \times 10^{-5})T^2$ [T in °C] [33]. External reference signals used for calibration of the correlation spectra were those of 2,2-dimethyl-2-silapentanesulfonic acid (DSS) for the carbon axis in the $^1H-^{13}C$ spectra ($^{13}C/^1H = 0.251449530$) and the NH_3 signal for the nitrogen axis in $^1H-^{15}N$ spectra ($^{15}N/^1H = 0.101329118$) [34].

Spectral processing was carried out using either the NMRPipe/NMRDraw [35] or VNMR [36] and analyzed with XEASY [37].

Construction of the Initial Peptide–SDS Complex

MD simulations were carried out with the parm99 force field in AMBER8.0 package [38]. Preparation of the SDS micelle was initiated by the construction of a single molecule of SDS based on the parameters taken from the literature [39,40]. The individual dodecyl sulfate was built in united-atoms presentation, with all bonds in the *trans* configuration. As is known, at room temperature, a micelle of SDS is formed by 60–70 monomers [41,42]. The initial micelle built by us contained 60 monomers of SDS. An innermost methyl group in each of the hydrophobic tails was placed at the apex of a 'buckyball' with a radius of 3.5 Å, with the remainder

DOI: 10.1002/psc

of the monomer extending outward. The paraffinic radius of 16.8 Å is in good agreement with the experimental one. The choice of 60 monomers for micelle building seems to be adequate for computer simulations, because the micelle is large enough to mimic all its physical properties and allows limiting calculational power. The initial model of the SDS micelle was then subjected to minimization, at first *in vacuo* and afterwards in aqueous solution. The initial solvent configuration around the micelle was obtained by filling a cubic box with water molecules. The overall box size was enlarged by about 8 Å in each direction. As a result, 7126 water molecules were added, bringing the total number of atoms in the system to 22 458. Finally, a 1 ns simulation was carried out in order to equilibrate the density of the entire system. The final density was 1.0080 g/ml (the experimental density of the SDS/water system is estimated as 1.0093 g/ml) [39].

Previous studies of the AVP–lipids interactions [23] showed that the side chains of Phe^3, Gln^4 and Pro^7 as well as the disulfide bridge are immersed in the nonpolar phase, whereas the side chains of Tyr^2, Asn^5, Arg^8 and Gly^9–NH_2 are in the aqueous phase. Thus, AVP was inserted into the micellar core in accordance with earlier investigations. In the case of MT, we decided to act in the same way, despite the fact that Ile^8 is a nonpolar residue in contrast to Arg^8. Three SDS molecules and three Na^+ counter-ions were deleted to create space for the peptide. The chloride ions were added to neutralize the entire system. The initial simulations were carried out at 301 K under constant pressure with constraints ($f = 20$ kcal/(mol × Å^2)) for distances between hydrophobic chains of SDS molecules and hydrophobic residues of the peptide, having in view the anchoring of the peptide in the hydrophobic part of the micelle. The final density of the system with the peptide was 1.0086 and 1.0064 g/ml for AVP and MT, respectively.

After equilibration, the MD with time-averaged (TAV) distance and dihedral angle restraints derived from the NMR spectroscopy was made. The interproton distances were restrained with the force constants $f = 20$ kcal/(mol × Å^2), and the dihedral angles with $f = 2$ kcal/(mol × rad^2). The improper dihedral angles centered at the C_α atoms were restrained with f = 50 kcal/(mol × rad^2). The geometry of the peptide groups was kept fixed according to the NMR data ($f = 50$ kcal/(mol × rad^2)). During MD simulation with TAV, an 8 Å cutoff radius was chosen. The MD simulations were carried out at 301 K in a periodic box of constant volume, with the particle-mesh Ewald (PME) procedure. The time step was 2 fs. The total duration of the run was 4 ns. The coordinates were collected every 2000th step. The conformations obtained during the last 800 ps of simulation were considered in further analysis. As a result, 200 conformations for each peptide were presented.

The interproton distances used in TAV were calculated by the CALIBA algorithm of the DYANA [43] program. The backbone $^3J_{NHH\alpha}$ coupling constants were converted to backbone torsion angle ϕ constraints according to the following rules: $^3J_{NHH\alpha} < 6$ Hz constrained the ϕ angle to the range of -90° to -30°, 6 Hz $< {}^3J_{NHH\alpha} < 8$ Hz constrained to the range of -120° to -60°, and $^3J_{NHH\alpha} > 8$ Hz constrained to the range of -140° to -100° [44].

The results obtained were analyzed using the Carnal and Ptraj programs from the AMBER [38] package. To find the peptide–micelle interactions, the radial distribution functions (RDFs) between the amino acid side chains and the negatively charged groups of SDS molecules and between the amino acid side chains and the SDS micelle hydrophobic core atoms were calculated. The data were averaged over the last 800 ps of MD simulation. To evaluate the interactions between the peptide and the water molecules, the hydration numbers were also calculated. The hydration number is an integral RDF that shows how many water molecules are located near a selected amino acid residue. Two sets of hydration numbers were calculated for the investigated SDS micelle/peptide systems: one for the heavy atoms of the amino acid side chains, and the other for the backbone carbonyl oxygen atoms of each amino acid residue. The first water shell was detected at less than 3.5 Å. Most of the residues also possess a well-defined second water shell (<5.0 Å). In the case of a lack of the isolated first water shell, the RDFs were integrated to 5.0 Å. The data were averaged over the last 800 ps of MD simulation.

Molecular structures were drawn and analyzed with the graphic programs RASMOL [45] and MOLMOL [46].

RESULTS AND DISCUSSION

NOE Effects, $^3J_{NHH\alpha}$ Coupling Constants, and Temperature Coefficients

The NMR spectra of both peptides in SDS micelle display only one proton resonance set, which reveals a reduced conformational space of the peptides. The proton chemical shifts of AVP and MT are summarized in Tables 1 and 2. The following number of interproton interactions on the NOESY spectra were found: 128 and 170 for AVP and MT, respectively. The number of interproton interactions in SDS micelle is higher than in aqueous solution [20] (see Part I), which may indicate a close structural compactness and lower flexibility.

The presence of all $d_{H\alpha-NH}(i, i+1)$ resonances indicate the *trans* peptide bonds. However, between Cys^1 and Tyr^2 of AVP, $d_{H\alpha-H\alpha}(i, i+1)$ connectivity characteristic of the *cis* peptide bond is seen in the NOESY spectrum (Figure 1). The *cis* peptide bond formation is probably due to the interactions of the disulfide bridge and Tyr^2 side chain with a hydrophobic part of the SDS micelle. Lack of exchange cross-peaks in the ROESY spectrum and only one cross-peak set eliminate the possibility of *cis*/*trans* isomerization across the Cys^1–Tyr^2 peptide bond for AVP in the SDS micelle.

In the case of isomerization across a X–Pro peptide bond, the sequential connectivity $H_\alpha(X)$–$H_\delta(Pro)$ confirms the *trans* peptide bond. However, in the case of AVP, this connectivity is not observed in the NOESY spectrum. Therefore, the *trans* Cys^6–Pro^7 peptide bond of AVP was confirmed by the carbon chemical shifts of C_β and C_γ. It is known that the signals of C_β and C_γ of Pro are found at 30.5 ± 0.6 and 25.2 ± 0.5 ppm for the *trans* and 32.2 ± 0.4 and 23.4 ± 0.3 for the *cis* isomer, respectively [47]. The carbon chemical shifts of C_β and C_γ of Pro^7 found at 30.7 and 25.7 ppm for AVP and at 30.9 and 24.9 ppm for MT indicate the *trans* Cys^6–Pro^7 peptide bond.

DOI: 10.1002/psc

Table 1 Proton chemical shifts, the amide proton temperature coefficients, and the vicinal coupling constants of AVP in SDS-d_{25} micelle solution at 28 °C

Residue	Proton chemical shifts (ppm)						$-\Delta\delta/\Delta T$ (ppb/K)	$^3J_{NHH\alpha}$ (Hz)
	NH	Hα	Hβ	Hγ	Hδ	Others		
Cys[1]		4.02	3.12					
Tyr[2]	8.62	4.16	2.63; 2.78			$H_{2,6}$ 6.70	4.6	
Phe[3]	7.95	4.87	3.09; 3.55			$H_{2,6}$ 7.36; $H_{3,5}$ 7.56; H_4 7.22	4.9	9.7
Gln[4]	8.76	4.03	2.14; 2.21	2.46		ε-NH_2 6.70	4.5	
Asn[5]	8.45	4.88	2.88			δ-NH_2 6.83; 7.53	6.2	9.5
Cys[6]	8.35	4.82	3.18;3.53				3.9	
Pro[7]	—	4.40	2.02; 2.40	2.08	3.59; 4.35		—	
Arg[8]	8.08	4.48	1.92; 2.12	1.74	3.27	ε-NH_2 7.21	2.9	9.6
Gly[9]	8.02	3.95; 4.01					2.3	

Table 2 Proton chemical shifts, the amide proton temperature coefficients, and the vicinal coupling constants of MT in SDS-d_{25} micelle solution at 28 °C

Residue	Proton chemical shifts [ppm]						$-\Delta\delta/\Delta T$ (ppb/K)	$^3J_{NHH\alpha}$ (Hz)
	NH	Hα	Hβ	Hγ	Hδ	others		
Cys[1]		4.20	2.97; 3.77					
Tyr[2]	8.84	4.59	2.92; 3.14			$H_{2,6}$ 6.88; $H_{3,5}$ 7.28	7.9	
Ile[3]	7.78	4.35	2.21	1.40; 1.49	0.99		1.2	8.8
Gln[4]	8.51	3.95	2.15; 2.32	2.45			3.9	5.9
Asn[5]	8.58	4.54	2.86			δ-NH_2 6.78; 7.53	8.3	
Cys[6]	8.30	4.92	2.97; 3.73				0.1	
Pro[7]	—	4.35	1.99; 2.43	2.02; 2.07	3.38; 4.02		—	
Ile[8]	7.84	4.36	2.17	1.32; 1.53	0.95		3.9	
Gly[9]	7.87	3.96					1.5	

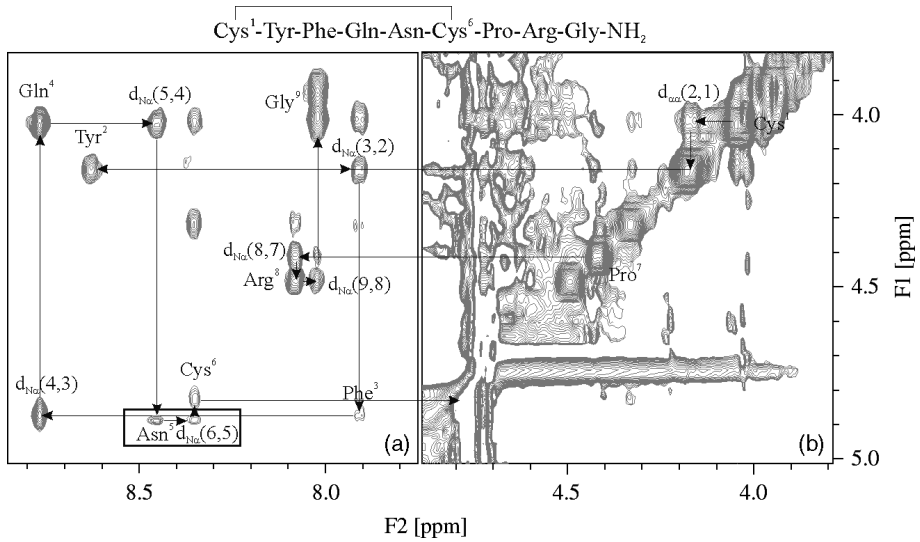

Figure 1 The fragment of NOESY spectrum of AVP in the SDS micelle (mixing time 200 ms) displays characteristic cross-peaks for *trans* or *cis* configuration of peptide bonds. Panel (A) corresponds to NH–Hα region, whereas panel (B) corresponds to Hα–Hα one. Fragment marked by square (panel A) is a fragment of ROESY spectrum (mixing time 200 ms), which is not observed in the NOESY.

DOI: 10.1002/psc

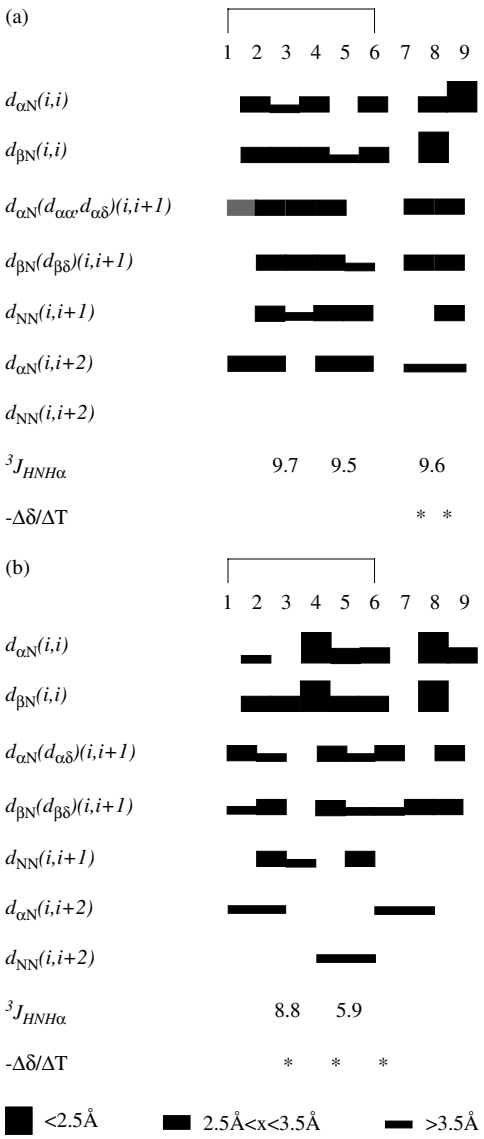

Figure 2 The NOE effects corresponding to their interproton distances and $^3J_{HNH\alpha}$ coupling constants. Temperature coefficients below 3 ppb/K are represented by asterisks. (a) AVP (gray color denotes $d_{H\alpha—H\alpha}$ NOE effect) and (b) MT.

The analysis of the NOE pattern allowed identification of regions of the peptides that assume reverse structures (Figure 2). In the case of AVP, the presence of the $d_{NH-NH}(i, i+1)$ and $d_{H\alpha-NH}(i, i+1)$, $(i, i+2)$ NOE effects (Figure 2(a)) indicate β-turns in the Cys^1–Gln^4, Phe^3–Cys^6, and Cys^6–Gly^9 fragments. In turn, the temperature coefficients of the amide protons of Arg^8 and Gly^9 (2.9 and 2.3 ppb/K) suggest the formation of hydrogen bonds NH^8–$CO^{5,6}$ and NH^9–$CO^{6,7}$, which stabilize γ- or β-turns in the *C*-terminal part of the molecule. It is also possible that these NH protons are involved in hydrogen bonds with water molecules, which might indicate that *C*-terminal part of AVP is exposed outside the SDS micelles. The $d_{NH-NH}(i, i+1)(i, i+2)$ and $d_{H\alpha—NH}(i, i+1)$, $(i, i+2)$ connections of MT demonstrate that both peptides create reverse structures in the Cys^1–Gln^4 and Cys^6–Gly^9 fragments. Moreover, the $d_{NH-NH}(i, i+2)$ effect shows the possibility of formation of β-turn within Ile^3–Cys^6. The temperature coefficients of the amide protons of Ile^3, Cys^6, and Gly^9 (1.2, 0.1 and 1.5 ppb/K, respectively) confirm the appearance of hydrogen bonds NH^3–CO^1, NH^6–$CO^{3,4}$, and NH^9–$CO^{6,7}$. In addition, the decreased temperature coefficients of these amide protons may suggest that these residues would be deeply buried in the micelles [48]. Over the 10–30 °C range, the amide protons of Ile^3, Gln^4, and Ile^8 are also involved in strong hydrogen bonds, but become broken at higher temperatures.

Analysis of the Calculated Structures

The structures of the peptides in SDS micelle are shown in Figure 3 and are aligned to their first coordinates using Cα atoms from the cyclic part of the molecules. The RMSD values for the ensemble of structures are about 0.1 Å in each case, thus suggesting a very similar structure of the cyclic part of the peptides.

In the case of the AVP in SDS micelle, the main structural elements are the βII′-turn at position 3,4; βI-turn at position 4,5 stabilized by HN^6–CO^3 hydrogen

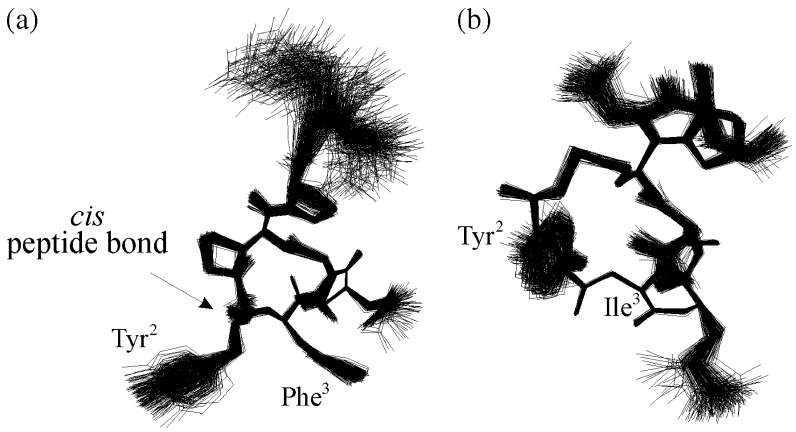

Figure 3 AVP and MT conformations obtained in the last 800 ps of MD simulations with time-averaged distances and dihedral angles restraints, (a) AVP and (b) MT. $RMSD_{1-6} = 0.124$ and 0.104 Å for C_α atoms, respectively.

DOI: 10.1002/psc

bond; and βIV-turn at position 5,6. The main difference between AVP structures in aqueous solution [20] (see Part I) and SDS micelle is the magnitude of the torsion angle ω around the Cys^1-Tyr^2 peptide bond. Namely, with AVP in the SDS micelle, the *cis* peptide bond is observed between Cys^1 and Tyr^2.

The analysis of MT structure shows that the type IV of the β-turn at position 3,4 is present. Besides, MT forms β-turn I′ or III′ at position 4,5. Additionally, the β-turn of type I or III at position 6,7 was found. MT possesses also a βIII-turn in the Cys^6–Gly^9 fragment stabilized by an HN^9–CO^6 hydrogen bond. The same structure was found in aqueous solution [20] (see Part I). Nevertheless, the frequency of its occurrence is much higher in the SDS micelle solution. Moreover, with MT the interactions between the side-chain amide group of Asn^5 and aromatic ring of Tyr^2 are observed.

Radial Distribution Functions and Hydration Numbers for AVP and MT in SDS Micelle

The analysis of the RDF values (Figures 4 and 5) and the hydration numbers (Table 3) for each residue of both peptides show that the main difference between both peptides is the location of the Tyr^2 side chain.

In AVP, the Tyr^2 side chain is immersed into the hydrophobic micelle core, whereas in MT it is exposed to the aqueous environment. Furthermore, the hydration number confirms that both the carbonyl oxygen and the side chain of Tyr^2 in MT are surrounded by water molecules. In turn, the Asn^5 side chain in both peptides shows a high hydration number; however, in AVP only the backbone oxygen atom of carbonyl group is hydrated, whereas in MT it is involved in intramolecular hydrogen bond, $\delta NH_2{}^5$–CO^5, and displays a low hydration number. Similarly, the hydration numbers of the oxygen atoms of Tyr^2 and Phe^3 in AVP suggest that either they are hidden from aqueous environment or are engaged in hydrogen bonds (HN^6–CO^3), respectively. In MT, the low hydration number calculated for the oxygen atom of Cys^6 suggests the existence of hydrogen bond, which is in agreement with the above-presented observations.

In AVP, strong interactions are noticed between Arg^8 and the sulfate of SDS. They are due to electrostatic interactions between a positively charged guanidine group of Arg^8 and a negatively charged group of the micelle head. Moreover, the negatively charged groups of SDS are close to the micelle–water interface, and thus the Arg^8 side chain is exposed to aqueous environment. Figure 6 shows final binding conformations of both peptides in the SDS micelle.

CONCLUSIONS

Recognition of peptide hormones by membrane-bound receptors can either occur directly from the

Table 3 Hydration numbers for each residue in SDS micelle/water system. The hydration numbers were averaged over the last 800 ps of simulations

AVP residues	Carbonyl oxygen			Side chains		
	First peak position (Å)	Integrated to (Å)	Hydration no.	First peak position (Å)	Integrated to (Å)	Hydration no.
Cys^1	3.14	4.34	1.02	3.51	3.89	0.39
Tyr^2	n	5.00	0	2.89	3.11	0.07
Phe^3	n	5.00	0	n	5.00	0.09
Gln^4	2.79	3.29	0.29	2.79	3.11	0.14
Asn^5	3.34	4.54	0.92	3.76	4.44	0.61
Cys^6	2.79	3.31	0.40	n	5.00	0.37
Pro^7	2.74	3.51	0.58	n	5.00	0.19
Arg^8	2.74	3.56	0.63	2.96	3.24	0.15
Gly^9	2.79	3.36	0.71	—	—	—
MT residues						
Cys^1	3.29	4.19	1.03	3.36	4.49	0.27
Tyr^2	2.76	3.51	0.74	3.66	4.14	0.66
Ile^3	2.76	3.81	0.57	n	5.00	0.06
Gln^4	2.74	3.31	0.30	3.74	4.11	0.66
Asn^5	n	5.00	0.19	3.76	4.61	1.00
Cys^6	n	5.00	0.09	n	5.00	0.02
Pro^7	2.76	3.96	0.42	n	5.00	0
Ile^8	2.79	3.81	0.80	3.99	4.14	0.29
Gly^9	2.76	3.71	0.88	—	—	—

n, not observed.

DOI: 10.1002/psc

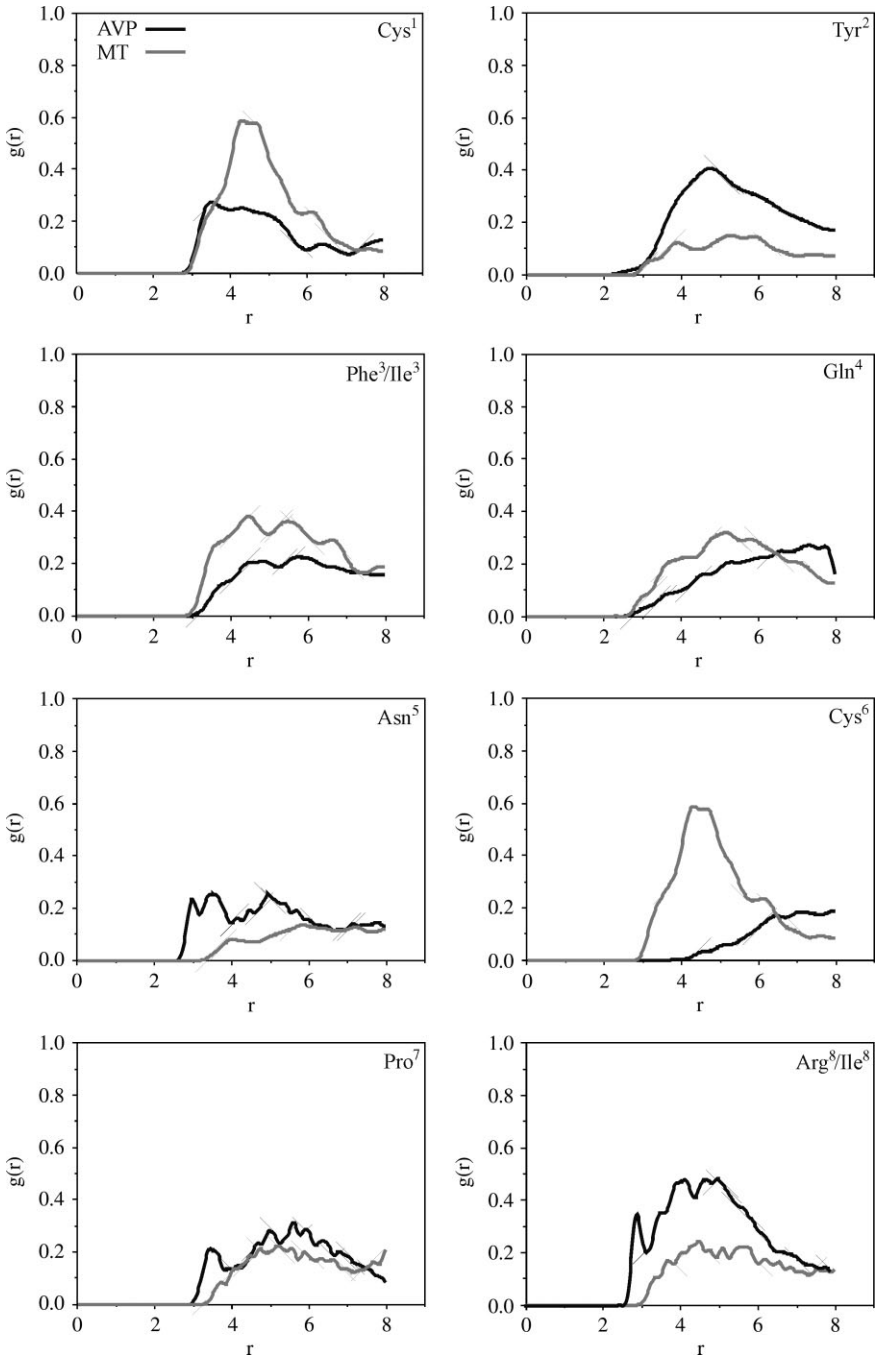

Figure 4 Radial distribution functions $g(r)$ between the sulfate head groups on SDS micelle and the side chain (heavy atoms) of each residue. The r parameter defines the distance in Å.

extracellular aqueous phase via collision with surface-exposed binding sites or by mediation by the statistically more favored preadsorption on the target cell membrane [21,22]. SDS is a simple model of a lipid bilayer and it is supposed that it can induce conformation of the peptide, which is bound by receptors. Thus, the analysis of conformational properties of both peptides in two solvents (H_2O/D_2O [20] and SDS-d_{25}/H_2O) seems to be reasonable. The parm99 force field in AMBER8.0 package has made possible the explicit solvent periodic calculations with water as a solvent, whereas the SDS micelle has been modeled in order to reflect the properties of the measurement environment in the best possible way.

The results of our investigations show that despite the high sequence homology between vasopressin and mesotocin, they do differ from each other with regard to the three-dimensional structure. Both possess β-turns in their cyclic part, which is in excellent agreement with earlier investigations of VP and OT-like peptides. In MT, the *C*-terminal fragment is involved in type III of β-turn stabilized by the HN^9–CO^6 hydrogen bond,

DOI: 10.1002/psc

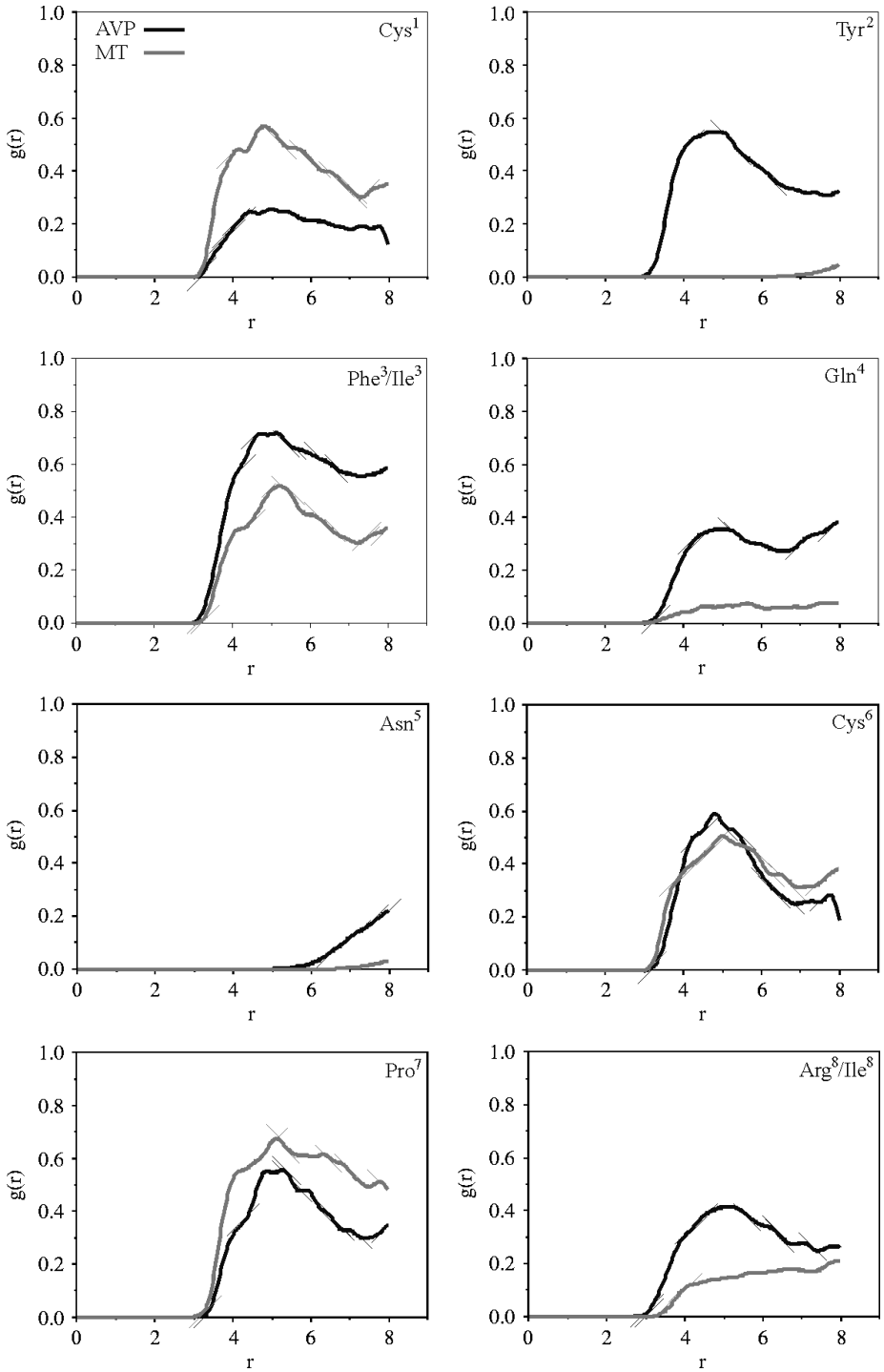

Figure 5 Radial distribution functions $g(r)$ between the micelle core and the side chain (heavy atoms) of each residue. The r parameter defines the distance in Å.

as in water [20]. As a result, the *C*-terminal tail of MT is more compact than in vasopressin. This suggests that the positively charged Arg at position 8 of the vasopressin promotes the extended conformation of the *C*-terminus. Moreover, the investigations in the SDS micelle have shown that the guanidinium group of Arg in AVP shows a tendency to be turned toward the hydrophilic environment. These suggestions are well grounded if we take into account the fact that the guanidinium of Arg^8 interacts with the extracellular (EL2) loop of receptor and as a result is exposed to the entrance of the binding pocket [49], which may confirm the extended conformation of the *C*-terminal tail of AVP.

The change of environment from water to SDS has influenced most of all the location of the side chains and flexibility of the peptides. To reduce the contact of the

DOI: 10.1002/psc

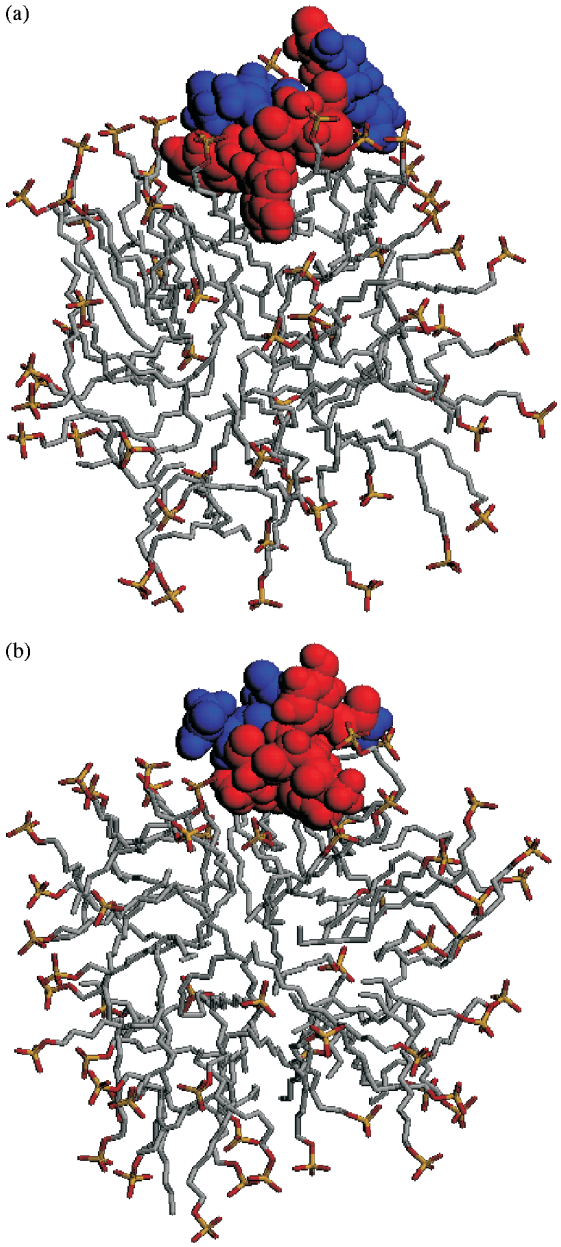

Figure 6 Final complexes of the peptides and SDS micelles, (a) AVP and (b) MT. Hydrophobic residues are colored in red and hydrophilic residues in blue.

hydrophobic side chains with aqueous phase, the Tyr^2 and Phe^3 residues of AVP approach each other in the aqueous solution [20] (see Part I). In turn, in the SDS micelle they are situated opposite to each other and are immersed into the hydrophobic part of the micelle. In MT in the SDS micelle, the side chain of Ile^3 shows a tendency to locate itself inside the cyclic part of the molecule. Moreover, it lies on a different side of the tocin ring plane than does Tyr [2]. This mutual arrangement of the Tyr^2 and Ile^3 side chains makes it impossible to immerse both hydrophobic side chains into the micelle core. Therefore, the more hydrophobic Ile is directed into the micelle core, whereas Tyr is exposed to the water phase. Furthermore, aromatic ring of Tyr^2 interacts with the side chain of Asn^5, which additionally maintains Tyr in the hydrophilic environment.

The SDS micelle restricts the conformational freedom of the peptides. It is manifested by the lack of multiplied set of cross-peaks, which are characteristic of the NMR spectra in aqueous solution. The existence of two sets of cross-peaks in the NMR spectra in water is due to *cis*/*trans* isomerization of the Cys^6–Pro^7 peptide bond. However, it should be emphasized that the Cys^1–Tyr^2 peptide bond of AVP in the SDS micelle adopts *cis* configuration, which has not been reported until now. This finding is very important with regard to designing new AVP analogs. An earlier investigated inactive AVP analog, [$DCys^1$, $MePhe^2$, $DMePhe^3$]AVP, showed only the tendency to *cis*/*trans* isomerization across the $DCys^1$–$MePhe^2$ peptide bond and in solution both major and minor isomers occurred. The percentage of conformation with the *cis* $DCys^1$–$MePhe^2$ peptide bond amounted to 40% in aqueous solution. However, the change of solvent from water to dimethyl sufloxide influenced also the change of position of *cis*/*trans* isomerization, and in DMSO the minor conformation had the *cis* peptide bond between Cys^6–Pro^7 [50].

A comparison of the AVP conformation obtained in this study with the AVP structures taken from the complexes of the 1–6 vasopressin–neurophysin [51], AVP–trypsin [52], AVP–receptor [53] and with free pressinoic acid shows large variations in the torsion angles. The closest similarity in the conformation of the cyclic part of peptide is between the AVP in water [20] and the free pressinoic acid ($RMSD_{C\alpha(1-6)} = 0.521$ Å) (Figure 7), where not only the backbone conformation is very similar but also the orientation of the aromatic residues is related. Moreover, the AVP in the SDS micelle and the 1–6 vasopressin-neurophysin have similar structures ($RMSD_{C\alpha(1-6)} = 0.961$ Å) (Figure 7), with the comparable orientation of the backbone and amino acid side chains. The AVP structure from the AVP–V_2 receptor complex differs considerably from those obtained in our investigations, especially in the cyclic part of the molecule ($RMSD_{C\alpha(1-6)} = 2.389$ and 2.267 Å for AVP in water [20] and SDS micelle, respectively) (Figure 7). Thus, the AVP peptide is flexible enough to adopt different conformations, which helps it to perform different biological functions.

In conclusion, we have determined the three-dimensional structures of very important physiological neurohormones, AVP and MT, in water [20] (see Part I) and in biological membrane environment. The analysis of the structural differences induced by the change of solution gives the basis to understand the mechanism of interactions of VP and OT-like hormones with their receptors. Moreover, the results should make easier the design of new analogs with appropriate biological activity, both for humans and animals. It is probably worth designing a new analog with the *cis* peptide bond

DOI: 10.1002/psc

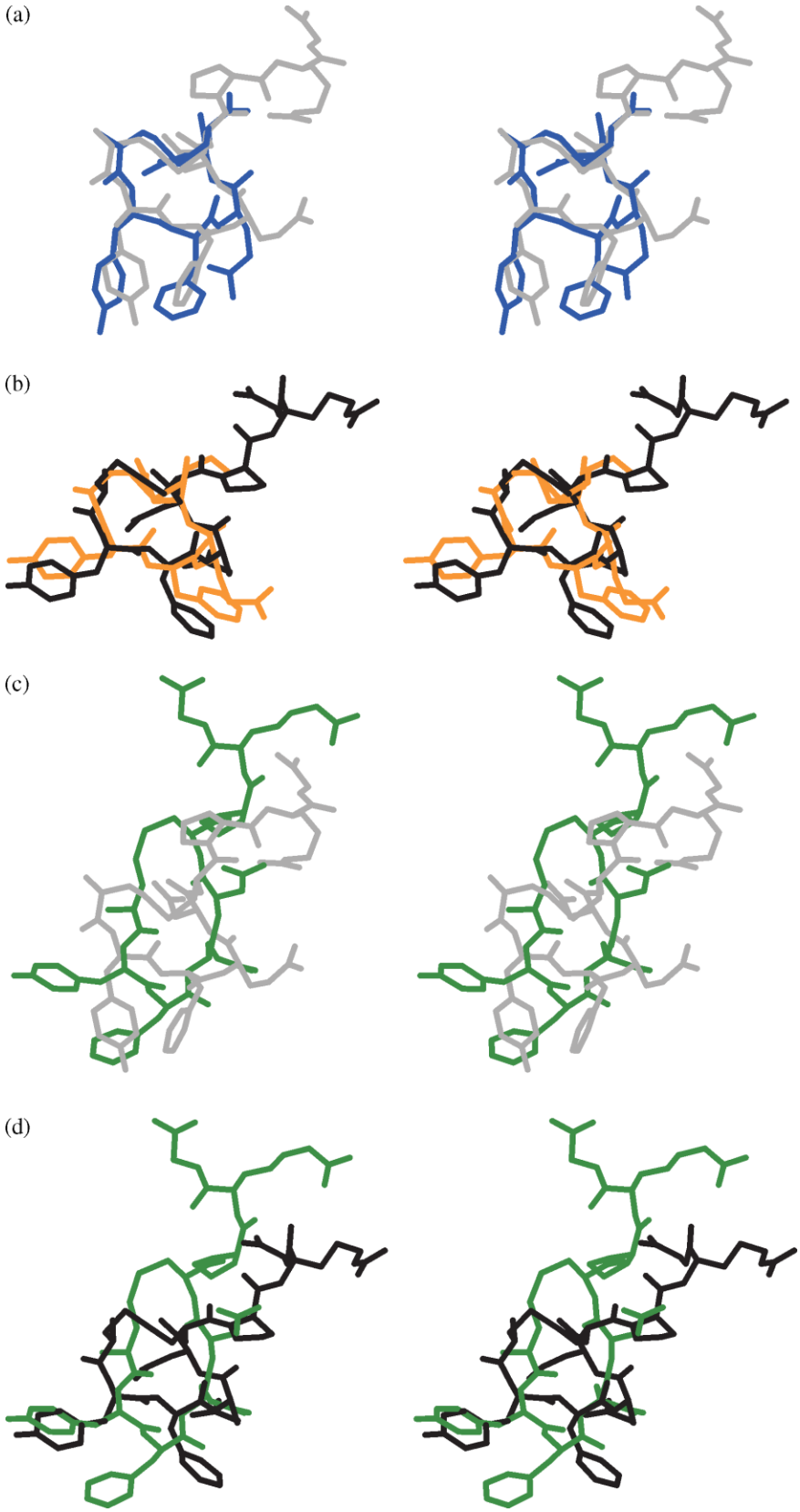

Figure 7 Stereo-view of a comparison of the conformation of AVP obtained in this study with AVP structures taken from the literature. (a) AVP in H_2O/D_2O (gray line) with pressinoic acid (blue line); (b) AVP in SDS-d_{25}/H_2O (black line) with complexes of 1–6 vasopressin-neurophysin (orange line); (c) AVP in H_2O/D_2O (gray line) with AVP–receptor (green line) and (d) AVP in SDS–d_{25}/H_2O (black line) with AVP–receptor (green line). $RMSD_{1-6} = 0.521$, 0.961, 2.389 and 2.267 Å for C_α atoms, respectively.

DOI: 10.1002/psc

between the first and the second amino acid position of AVP and to check biological activity of the modified peptide.

Acknowledgements

This work was supported by the Polish Scientific Research Committee Grant KBN 4 T09A 022 22 and DS 8372-4-0138-6 grants. The calculations were carried out in the Academic Computer Centre (TASK) in Gdańsk, Poland.

REFERENCES

1. Hoyle CHV. Neuropeptide families and their receptors: evolutionary perspectives. *Brain Res.* 1999; **848**: 1–25.
2. Bockaert J, Roy C, Rajerison R, Jard S. pecific binding of (3H) lysine-vasopressin to pig kidney plasma membranes. Relationship of receptor occupancy to adenylate cyclase activation. *J. Biol. Chem.* 1973; **248**: 5922–5931.
3. Luft FC, Steinberg H, Ganten U, Meyer D, Gless KH, Lang RE, Fineberg NS, Rascher W, Unger T, Ganten D. Effect of sodium chloride and sodium bicarbonate on blood pressure in stroke-prone spontaneously hypertensive rats. *Clin. Sci. (London)* 1988; **74**: 577–585.
4. Versteeg CA, Bohus B, de Jong W. Attenuation by arginine- and desglycinamide-lysine-vasopressin of a centrally evoked pressor response. *J. Auton. Nerv. Syst.* 1982; **6**: 253–262.
5. Jard S, Gaillard RC, Guillon G, Marie J, Schoenenberg P, Muller AF, Manning M, Sawyer WH. Vasopressin antagonists allow demonstration of a novel type of vasopressin receptor in the rat adenohypophysis. *Mol. Pharmacol.* 1986; **30**: 171–177.
6. Wilkinson MF, Kasting NW. The antipyretic effects of centrally administered vasopressin at different ambient temperatures. *Brain Res.* 1987; **415**: 275–280.
7. Wang Z, Young LJ, De Vries GJ, Insel TR. Voles and vasopressin: a review of molecular, cellular, and behavioral studies of pair bonding and paternal behaviors. *Prog. Brain Res.* 1998; **119**: 483–499.
8. Kendrick KM, Keverne EB, Baldwin BA. Intracerebroventricular oxytocin stimulates maternal behaviour in the sheep. *Neuroendocrinology* 1987; **46**: 56–61.
9. Berkowitz BA, Sherman S. Characterization of vasopressin analgesia. *J. Pharmacol. Exp. Ther.* 1982; **220**: 329–334.
10. van Ree JM, De Wied D. Effect of neurohypophyseal hormones on morphine dependence. *Psychoneuroendocrinology* 1977; **2**: 35–41.
11. Barberis C, Tribollet E. The vasopressin and oxytocin receptors in the central nervous system. *Crit. Rev. Neurobiol.* 1996; **10**: 119–154.
12. Stiffler DF, Roach SC, Pruett SJ. A comparison of the responses of the amphibian kidney to mesotocin, isotocin and oxytocin. *Physiol. Zool.* 1984; **57**: 63–69.
13. Jard S, Morel F. Actions of vasotocin and some if its analogues on salt and water excretion by the frog. *Am. J. Physiol.* 1963; **204**: 222–226.
14. Pang PKT, Sawyer WH. Renal and vascular responses of the bullfrog (Ram catesbeiana) to mesotocin. *Am. J. Physiol.* 1978; **235**: F151–F155.
15. Warburg MR. Hormonal effect on the osmotic, electrolyte and nitrogen balance in terrestrial amphibian. *Zool. Sci.* 1995; **12**: 1–11.
16. Gonzalez A, Smeets WJ. Distribution of vasotocin and mesotocin-like immunoreactivities in the brain of the South African clawed frog *Xenopus-laevis*. *J. Chem. Neuroanat.* 1992; **5**: 465–479.
17. Nojiri H, Ishida I, Miyashita E, Sato M, Urano A, Deguchi I. Cloning and sequence analysis of cDNA for neurohypopyseal hormones vasotocin and mesotocin for the hypothalamus of toad, *Bufo japonicus*. *Proc. Natl. Acad. Sci. U.S.A.* 1987; **84**: 3043–3046.
18. Acher R, Chauvet J, Chauvet MT, Grepg D. Phylogknie des hormones hypophysaires: isolement de la mksotocine: ([Ile8]-ocytocine) de la grenouille, intermkdiaire entre la [Ser', Hex]-ocytocine des poissons osseux et l'ocytocine des mammiferes. *Biochim. Biophys. Acta* 1964; **90**: 613–615.
19. Acher R. Neurohypohyseal peptide systems: processing machinery, hydroosmotic regulation adaptation and evolution. *Regul. Pept.* 1993; **45**: 1–13.
20. Sikorska E, Rodziewicz-Motowidło S. Conformational Studies of Vasopressin and Mesotocin Using NMR Spectroscopy and Molecular Modelling Methods. part I: studies in water: *J. Pept. Sci.* 2007; DOI:10.1002/psc.918.
21. Schwayzer RJ. In search of the 'bio-active conformation' – is it induced by the target cell membrane? *J. Mol. Recognit.* 1995; **8**: 3–8.
22. Mierke DF, Giragossian C. Peptide hormone binding to G-protein-coupled receptors: structural characterization via NMR techniques. *Med. Res. Rev.* 2001; **21**: 450–471.
23. Grzonka Z, Gwizdała E, Kasprzykowski F, Liwo A, Łankiewicz L, Łubkowska L, Galaktionov SG, Tseitin VM. Studies of the interaction of neurohypophyseal hormones with lipids. In *Peptides 1990*, Giralt E, Andreu D (eds.). ESCOM Science Publishers B.V. Leiden: The Netherlands, 1991; 488–489.
24. Tu AT, Lee J, Deb KK, Hruby VJ. Laser Raman spectroscopy and circular dichroism studies of the peptide hormones the mesotocin, vasotocin, lysine the vasopressin, and arginine the vasopressin. *J. Biol. Chem.* 1979; **254**: 3272–3278.
25. Bax A, Freeman R. Enhanced NMR resolution by restricting the effective sample volume. *J. Magn. Reson.* 1985; **65**: 355–360.
26. Kumar A, Ernst RR, Wüthrich K. A two-dimensional nuclear Overhauser enhancement (2D NOE) experiment for the elucidation of complete proton-proton cross relaxation networks in biological macromolecules. *Biochem. Biophys. Res. Commun.* 1980; **95**: 1–10.
27. Bothner-By AA, Stephens RL, Lee JM, Warren CD, Jeanloz RW. Structure determination of a tetrasaccharide: transient nuclear Overhauser effects in the rotating frame. *J. Am. Chem. Soc.* 1980; **106**: 811–813.
28. Bax A, Davis DG. Practical aspects of two-dimensional transverse NOE spectroscopy. *J. Magn. Reson.* 1985; **63**: 207–213.
29. Kay LE, Keifer P, Saarinen T. Pure absorption gradient enhanced heteronuclear single quantum correlation spectroscopy with improved sensitivity. *J. Am. Chem. Soc.* 1992; **114**: 10663–10665.
30. Kontaxis G, Stonehouse J, Laue ED, Keeler J. The sensitivity of experiments which use gradient pulses for coherence-pathway selection. *J. Magn. Reson., Ser. A* 1994; **111**: 70–76.
31. Bax A, Summers MF. Proton and carbon 13 assignments from sensitivity-enhanced detection of heteronuclear multiple-bond connectivity by 2D multiple quantum NMR. *J. Am. Chem. Soc.* 1986; **108**: 2093–2094.
32. Koźmiński W. The new active-coupling-pattern tilting experiment for an efficient and accurate determination of homonuclear coupling constants. *J. Magn. Reson.* 1998; **134**: 189–193.
33. Gottlieb HE, Kotlyar V, Nudelman A. NMR chemical shifts of common laboratory solvents as trace impurities. *J. Org. Chem.* 1997; **62**: 7512–7515.
34. Wishart DS, Bigam CG, Holm A, Hodges RS, Sykes BD. ^{1}H, ^{13}C and ^{15}N random coil NMR chemical shifts of the common amino acids. I. Investigations of nearest-neighbor effects. *J. Biomol. NMR* 1995; **5**: 67–81.
35. Delaglio F, Grzesiek S, Geerten WV, Zhu G, Pfeifer J, Bax A. NMRPipe: a multidimensional spectral processing system based on UNIX pipes. *J. Biomol. NMR* 1995; **6**: 277–293.
36. Varian, Nuclear Magnetic resonance Instruments, VnmrTM Software, Revision 5.3B 1/97.
37. Bartles C, Xia T, Billeter M, Günter P, Wütrich K. The program XEASY for the computer-supported NMR spectral analysis of biological macromolecules. *J. Biomol. NMR* 1995; **5**: 1–10.

38. Case DA, Darden TA, Cheatham TE III, Simmerling CL, Wang J, Duke RE, Luo R, Merz KM, Wang B, Pearlman DA, Crowley M, Brozell S, Tsui V, Gohlke H, Mongan J, Hornak V, Cui G, Beroza P, Schafmeister C, Caldwell JW, Ross WS, Kollman PA. *AMBER 8*. University of California: San Francisco, 2004.
39. Schweighofer KJ, Essman U, Berkowitz M. Simulation of sodium dodecyl sulfate at the water-vapor and water-carbon tetrachloride interfaces at low surface coverage. *J. Phys. Chem. B* 1997; **101**: 3793–3799.
40. Bruce CD, Berkowitz ML, Perera L, Forbes MDE. Molecular Dynamics Simulation of Sodium Dodecyl Sulfate Micelle in Water: Micellar Structural Characteristics and Counterion Distribution. *J. Phys. Chem. B* 2002; **106**: 3788–3793.
41. Jonsson B, Lindman B, Holmberg K, Kronberg B. *Surfactants and Polymers in Aqueous Solution*. John Wiley & Sons: West Sussex, 1998; 53.
42. Chen JM, Su TM, Mou CY. Size of sodium dodecyl sulfate micelle in concentrated salt solutions. *J. Phys. Chem.* 1986; **90**: 2418–2421.
43. Güntert P, Mumenthaler C, Wüthrich K. Torsion angle dynamics for NMR structure calculation with the new program DYANA. *J. Mol. Biol.* 1997; **273**: 283–298.
44. Pardi A, Billeter M, Wüthrich K. Calibration of the angular-dependence of the amide proton-C-alpha proton coupling-constants, $^3J_{HNH\alpha}$, in a globular protein – use of $^3J_{HNH\alpha}$ for identification of helical secondary structure. *J. Mol. Biol.* 1984; **180**: 741–751.
45. Sanchez-Ferrer A, Nunez-Delicado E, Bru R. Software for viewing biomolecules in three dimensions on the internet. *Trends Biochem. Sci.* 1995; **20**: 286–288.
46. Koradi R, Billeter M, Wüthrich K. MOLMOL: a program for display and analysis of macromolecular structures. *J. Mol. Graphics* 1996; **14**: 52–55.
47. Dorman DE, Bovey FA. Carbon magnetic resonance spectroscopy. The spectrum of proline in oligopeptides. *J. Org. Chem.* 1973; **38**: 2379–2383.
48. Kohno T, Kobayashi K, Maeda T, Sato K, Takashima A. Three-dimensional structures of the amyloid ß peptide (25–35) in membrane-mimicking environment. *Biochemistry* 1996; **35**: 16094–16104.
49. Ślusarz MJ, Giełdoń A, Ślusarz R, Ciarkowski J. Analysis of interactions responsible for vasopressin binding to human neurohypophyseal hormone receptors – molecular dynamics study of the activated receptor–vasopressin–Gα systems. *J. Pept. Sci.* 2006; **12**: 180–189.
50. Sikorska E, Ślusarz MJ, Lammek B. Conformational studies of vasopressin analogues modified with N-methylphenylalanine enantiomers in dimethylsulfoxide solution. *Biopolymers* 2006; **82**: 603–614.
51. Wu CK, Hu B, Rose JP, Liu ZJ, Nguyen TL, Zheng TL, Breslow E, Wang BC. Structures of an unliganded neurophysin and its the vasopressin complex: implications for binding and allosteric mechanisms. *Protein Sci.* 2001; **10**: 1869–1880.
52. Ibrahim SB, Pattabhi V. Trypsin inhibition by a peptide hormone: crystal structure of trypsin-vasopressin complex. *J. Mol. Biol.* 2005; **348**: 1191–1198.
53. Czaplewski C, Kaźmierkiewicz R, Ciarkowski J. Molecular modeling of the human the vasopressin V2 receptor/agonist complex. *J. Comput. Aided Mol. Des.* 1998; **12**: 275–287.

DOI: 10.1002/psc